

Antiferromagnetic phase transitions in an ordered Pt₃Fe(111) film studied by neutron diffraction

V. V. Krishnamurthy, I. Zoto, and G. J. Mankey

Center for Materials for Information Technology and Department of Physics and Astronomy, University of Alabama, Tuscaloosa, Alabama 35487-0209, USA

J. L. Robertson

Condensed Matter Sciences Division, Oak Ridge National Laboratory, Oak Ridge, Tennessee 37831-6393, USA

S. Maat and Eric E. Fullerton

Hitachi Global Storage Technologies, San Jose Research Center, 650 Harry Road, San Jose, California 95120, USA

I. Nwagwu and J. K. Akujieze

Department of Chemistry and Physics, Chicago State University, Chicago, Illinois 60628, USA

(Received 10 October 2003; revised manuscript received 17 February 2004; published 30 July 2004)

Neutron diffraction has been used to investigate the critical behavior at the onset of antiferromagnetic phase transitions in a (111) oriented Pt₇₃Fe₂₇ film grown on an *a*-axis oriented sapphire (α -Al₂O₃) substrate. As in the bulk, there is an antiferromagnetic reorientation transition from the $Q_1=2\pi/a(1/2, 1/2, 0)$ phase to the $Q_2=2\pi/a(1/2, 0, 0)$ phase upon cooling. The temperature dependence of the integrated intensity of the $(1/2, 1/2, 0)$ and the $(1/2, 0, 0)$ antiferromagnetic Bragg peaks yielded the Néel temperature of 160.25 ± 0.2 K and a reorientation transition temperature of 95 ± 0.2 K. The magnetization critical exponent β is found to be 0.368 ± 0.013 for the Q_1 phase and 0.37 ± 0.02 for the Q_2 phase. These critical exponents are in excellent agreement with the predictions of the 3*d* Heisenberg universality class. A comparison of the transition temperatures and the exponents in the film and in single crystal at the same alloy composition is presented.

DOI: 10.1103/PhysRevB.70.024424

PACS number(s): 75.25.+z, 75.40.Cx, 75.70.-i, 75.50.Ee

Magnetic thin films can exhibit structural and magnetic behaviors that are different from bulk due to strain and changes in grain size induced by the substrate. Compared to ferromagnetic films, antiferromagnetic (AF) films are less studied. Presently, there is a growing interest to investigate AF films to gain insight into the modifications in their magnetic and structural properties. Antiferromagnetically ordered thin films are currently used as pinning layers for creating unidirectional anisotropy in ferromagnetic layers in magnetic read head sensors and may be used in media applications as well. Antiferromagnets, such as IrMn, PtMn and NiO, are typically used as pinning layers for elemental ferromagnets, such as Co and Fe. Metallic antiferromagnets consisting of transition metals are more attractive in such applications because of their higher exchange bias field and improved thermal stability. Neutron diffraction measurements in epitaxial thin films can yield unique information on the magnetic ordering, such as the AF structure, properties of magnetic phase transitions, and the thermal evaluation of the order parameter. These measurements enable the understanding of the correlation between structural and magnetic properties.

Critical exponents enable us to understand antiferromagnetic phase transitions from a generalized point of view.¹ For continuous phase transitions, including magnetic phase transitions, the critical exponents and the scaling functions depend only on global properties, such as the dimensionality of the order parameter, the range of exchange interactions, and the dimensionality of the system. These three parameters define the type and dimensionality of the universality class. The

Heisenberg universality class, which describes the critical behavior of isotropic ferromagnets and antiferromagnets, has a three-component order parameter. The XY universality class, which describes ferromagnets or antiferromagnets with planar anisotropy, has a two-component order parameter. The Ising universality class, which describes the critical behavior of anisotropic ferromagnets and antiferromagnets, has a single-component order parameter. Each of these models can be used to describe the magnetic behavior of 1D (chains), 2D (planes), or 3D solids.

A few alloys of Pt with the 3*d* transition metals that order in Cu₃Au (*L*₁₂) type cubic structure or in CuAu (*L*₁₀) type tetragonal structure exhibit AF ordering.^{2,3} Atomically ordered Pt₃Fe crystallizes in the *L*₁₂ phase and exhibits long-range AF ordering with a Néel temperature (T_N) of 160 K.² Neutron diffraction measurements of ordered Pt₃Fe films that are epitaxially grown on MgO(110) and *a*-axis-oriented sapphire (α -Al₂O₃) substrates show that these films exhibit AF ordering below $T_{N1}=160$ K with a wave vector $Q_1=2\pi/a(1/2\ 1/2\ 0)$, in which the magnetic moments of Fe align antiferromagnetically in alternating ferromagnetic sheets in the (110) plane. With the decrease of temperature, the intensity of the Q_1 peak decreases and another AF phase with a wave vector $Q_2=2\pi/a(1/2\ 0\ 0)$ appears below $T_{N2}=100$ K only in near-stoichiometric-grown Pt₃Fe films on an *a*-axis sapphire substrate. The absence of the Q_2 phase for films grown onto MgO (110) was attributed to strain.⁴ It has been argued that the low-temperature AF phase occurs upon a reorientation of the Fe spins, which produces alternating

ferromagnetic sheets in the (100) plane.² Although no magnetic Bragg peaks of the low-temperature Q_2 phase could be detected for Pt_3Fe films grown onto MgO (110) with neutron diffraction, both superconducting quantum interference device (SQUID) magnetometry and ferromagnetic resonance (FMR) showed clear evidence of the Q_2 phase in exchange biased FePt_3/Fe bilayer films on MgO (110) substrates under similar growth conditions.⁵ Presently, the origin of the two antiferromagnetic phases is debated in the context of different models, which include the degeneracy of the Fermi surface⁶ and the nesting of electron and hole Fermi surfaces.⁷ Moreover, recent inelastic neutron scattering experiments of Pt_3Fe single crystal showed magnetic excitations around $(1/2\ 0\ 0)$ even above T_{N2} , where no magnetic Bragg peaks are observed. This lead to the hypothesis that above T_{N2} , spins order in the Q_1 phase, but fluctuate with a strong $(1/2\ 0\ 0)$ correlation.⁸ It has been suggested that this correlation then freezes below T_{N2} into a noncollinear spin structure giving rise to both $(1/2, 0, 0)$ and $(1/2, 1/2, 0)$ AF Bragg peaks.⁸ It is desirable to have a better understanding of the magnetic phase transitions in Pt_3Fe . Here, we report neutron diffraction study of the antiferromagnetic phase transitions in an epitaxial Pt_3Fe film grown on $\alpha\text{-Al}_2\text{O}_3$ substrate. The results show that the critical behavior of the order parameter in the film at the two AF transitions follows the predicted behavior of the $3d$ Heisenberg model.

A 280-nm film of (111) oriented and chemically ordered $\text{Pt}_{73}\text{Fe}_{27}$ was grown on an $\alpha\text{-Al}_2\text{O}_3$ substrate using magnetron sputtering as reported for the sample S1 in Ref. 4. A 1-nm-thick Fe layer followed by a 2-nm-thick Pt_3Cr layer were used as seed layers for the $\text{Pt}_{73}\text{Fe}_{27}$ layer on the $\alpha\text{-Al}_2\text{O}_3$ substrate. The chemical order was achieved by heating the substrate to 750°C during growth. The film was characterized by x-ray diffraction, which yielded the in- and out-of-plane lattice constants of 3.864 \AA and 3.872 \AA , respectively, and confirmed the existence of twins that are rotated 60° with respect to each other.⁴ The lattice constant is in excellent agreement with the value of 3.87 \AA reported for bulk Pt_3Fe , and therefore the film grown on $\alpha\text{-Al}_2\text{O}_3$ is essentially free from lattice strain. Rutherford backscattering was used to verify the composition with an uncertainty of 1% (Ref. 4). The $(11\text{-}2)$ in-plane lattice vectors of $\text{Pt}_{73}\text{Fe}_{27}$ twins are rotated 6° degrees with respect to the in-plane c -axis of the sapphire substrate. Neutron diffraction measurements were performed using the HB1 triple axis spectrometer of the High Flux Isotope Reactor Facility at Oak Ridge National Laboratory, Oak Ridge, Tennessee. Neutrons with a wavelength of 2.35 \AA were selected by a vertically focusing pyrolytic graphite (002) monochromator. A pyrolytic graphite filter was used to suppress the contribution from higher-order harmonics of the neutron wavelength. A pyrolytic graphite (002) analyzer crystal was used to reduce the background and reject neutrons that were inelastically scattered by the substrate. The collimation was open $(48')$ -monochromator- $40'$ -sample- $40'$ -analyzer- $120'$ - He^3 detector. The sample temperature was controlled in the range of $10\text{--}200\text{ K}$ using a closed-cycle Helium refrigerator. The temperature stability was better than $\pm 0.1\text{ K}$ in the range of $75\text{--}175\text{ K}$.

Diffraction peaks were measured as a function of tem-

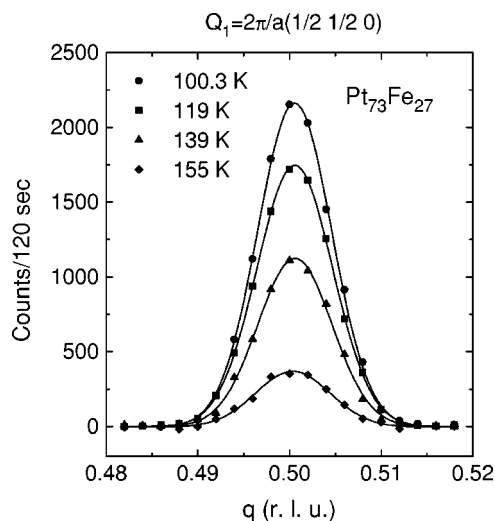


FIG. 1. The scattering intensity of the antiferromagnetic $(1/2\ 1/2\ 0)$ Bragg peak at selected temperatures in the $\text{Pt}_{73}\text{Fe}_{27}$ film.

perature from 100 to 175 K for the Q_1 phase and in the range of $75\text{--}100\text{ K}$ for the Q_2 phase with 2 K temperature intervals to investigate the phase transitions. The Bragg scattering peaks have line widths associated with the resolution of the instrument and with the mosaic spread of the antiferromagnetic domains. The data was fitted by a Gaussian for quantifying the antiferromagnetic order and a q -independent term for the instrumental background. Figure 1 displays the $(1/2\ 1/2\ 0)$ Bragg peak intensity as a function of q for selected temperatures. Figure 2 displays the $(1/2\ 0\ 0)$ Bragg peak intensity as a function of the reciprocal lattice vector q for selected temperatures. In both cases, the integrated peak intensity decreases as the temperature is increased to approach the transition temperature.

In a magnetically ordered state, the spins of the magnetic atoms in a solid are correlated for an infinite time. Then, the

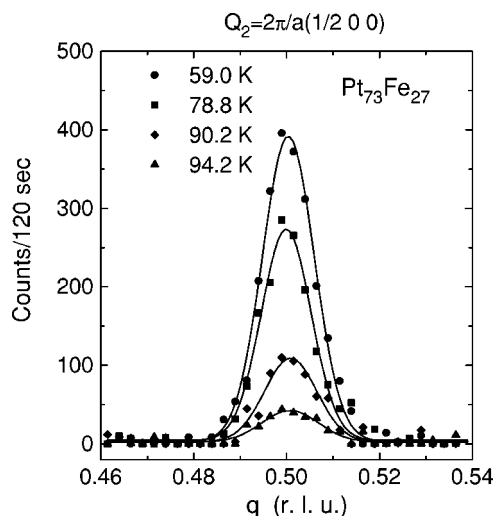


FIG. 2. The scattering intensity of the antiferromagnetic $(1/2\ 0\ 0)$ Bragg peak at selected temperatures in the $\text{Pt}_{73}\text{Fe}_{27}$ film.

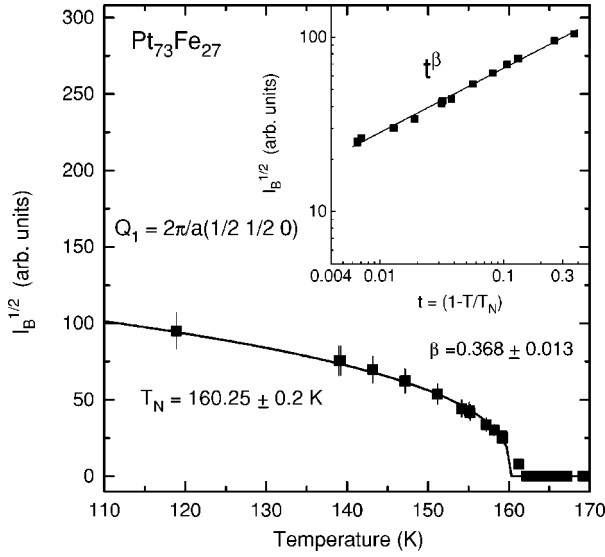


FIG. 3. The square root of the integrated scattering intensity $I_B^{1/2}$ of the antiferromagnetic $(1/2\ 1/2\ 0)$ Bragg peak as a function of temperature showing the onset of Néel order at ~ 160 K in the $\text{Pt}_{73}\text{Fe}_{27}$ film. Inset shows the log-log plot of $I_B^{1/2}$ versus reduced temperature t . The solid line is a fit by Eq. (3).

scattering of neutrons by the crystal is purely elastic. The differential cross section for elastic magnetic neutron scattering is given by⁹

$$\left(\frac{d\sigma}{d\Omega}\right) = \frac{1}{N} \frac{2\pi^3}{v_0} \sum_{TM} \delta(Q - \tau_M) |F_{M\perp}(\tau_M)|^2, \quad (1)$$

where N is the number of magnetic ions, v_0 is the neutron initial velocity, Q is the scattering vector, $F_{M\perp} = Q \times F_M \times Q$ is the magnetic structure factor, F_M is the structure factor of the unit cell, $\tau_M = \tau \pm k$ is the reciprocal lattice vector of the magnetic structure, τ is the propagation vector of the crystal structure, and k is the propagation vector of the magnetic structure. The magnetic Bragg reflection occurs for $Q = \tau_M$. The integrated intensity of a magnetic Bragg reflection (hkl) is given by¹⁰⁻¹²

$$I_B(hkl) = C_j A(\theta_B) \gamma_c \langle O_M^2 \rangle |F_M|^2, \quad (2)$$

where C is a constant that depends on the resolution of the instrument, j is the multiplicity of the reflection, $A(\theta_B)$ is an angle factor that depends on the method of measurement, θ_B is the Bragg scattering angle, $\gamma_c = -0.27 \times 10^{-12}$ cm is the neutron-electron coupling constant, $\langle O_M^2 \rangle$ is the orientation factor which is given by $\langle \sin^2 \Phi \rangle$ where Φ is the angle between the magnetization vector and the scattering plane, and F_M is the magnetic structure factor, which is proportional to the thermal average of the magnetic moment per Fe atom.

Figure 3 shows the square root of the integrated intensity of the AF $(1/2, 0, 1/2)$ Bragg peak as a function of temperature. The onset of long-range AF order is seen at about 160 K. The square root of the Bragg peak intensity ($I_B^{1/2}$), which is proportional to the sublattice magnetization M , i.e., order parameter, has been fitted to a power-law function:

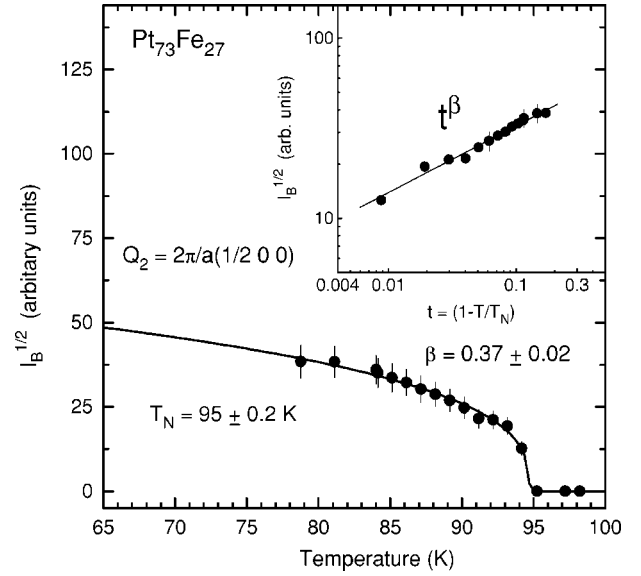


FIG. 4. The square root of the integrated scattering intensity $I_B^{1/2}$ of the antiferromagnetic $(1/2\ 0\ 0)$ Bragg peak as a function of temperature showing the onset of Néel order at ~ 95 K in the $\text{Pt}_{73}\text{Fe}_{27}$ film. Inset shows the log-log plot of $I_B^{1/2}$ versus reduced temperature t . The solid line is a fit by Eq. (3).

$$I_B^{1/2} \sim M = M_0 t^\beta, \quad (3)$$

where $t = (1 - T/T_N)$ is the reduced temperature and β is the critical exponent.¹³ The values of the critical exponent and the Néel temperature have been determined by the following method. First, the reduced temperature t is calculated for a value of T_X . Then $I_B^{1/2}$ is plotted as a function of t in a log-log plot as shown in the inset in Fig. 2. The data is fitted by Eq. (3) to extract the error. The procedure is repeated for different values of T_X to obtain an error versus T_X curve that has the shape of a parabola. The value of T_X with minimum in error yielded T_N of the transition. The exponent β is also obtained with a similar procedure. The solid line superimposed over the data in Fig. 3 is obtained for the best fitted values of the Néel temperature $T_{N1} = 160.25 \pm 0.2$ K and the critical exponent, $\beta = 0.368 \pm 0.013$. The Néel temperature of 160 K reported for a $\text{Pt}_{73.3}\text{Fe}_{26.7}$ single crystal^{2,8} from neutron diffraction is within the uncertainty of the fitted value. The above value of β corresponds to the exponent expected for the 3D Heisenberg model.¹⁴

Figure 4 shows the square root of the integrated intensity of the AF $(1/2, 0, 0)$ Bragg peak as a function of temperature. The onset of long-range antiferromagnetic order is seen at $T \sim 95.0 \pm 0.2$ K. The order parameter, which is proportional to the square root of the intensity ($I_B^{1/2}$), has been fitted to a power-law function defined in Eq. (3). The Néel temperature T_{N2} and the exponent β have been determined by the procedure described above. Such an analysis yielded the Néel temperature $T_{N2} = 95.0 \pm 0.2$ K and the critical exponent, $\beta = 0.37 \pm 0.02$ for the Q_2 phase. The above value of T_{N2} is 14% smaller than the transition temperature reported for $\text{Pt}_{73.3}\text{Fe}_{26.7}$ single crystal from neutron diffraction.^{2,8} The value of the critical exponent for the Q_2 antiferromagnetic phase also agrees with the critical exponents of the 3D

TABLE I. Comparison of the experimental values of the critical exponent β in $\text{Pt}_{73}\text{Fe}_{27}$ film and in a $\text{Pt}_{73.3}\text{Fe}_{26.7}$ single crystal determined from neutron diffraction with the critical exponent of the $3d$ Heisenberg model from various theoretical calculations, of the $3d$ XY model and of the $3d$ Ising model.

Reference	Model	Method	Critical exponent β
This work		Neutron diffraction, $Q_1=(1/2, 1/2, 0)$	0.368 ± 0.13
($\text{Pt}_{73}\text{Fe}_{27}$ film)		Neutron diffraction, $Q_2=(1/2, 0, 0)$	0.37 ± 0.02
Ref. 2		Neutron diffraction, $Q_1=(1/2, 1/2, 0)$	0.40 ± 0.03
($\text{Pt}_{73.3}\text{Fe}_{26.7}$ single crystal)		Neutron diffraction, $Q_1=(1/2, 0, 0)$	0.39 ± 0.03
Ref. 14	$3d$ Heisenberg	Monte Carlo+High temp. expansion	0.3689 ± 0.0003
Ref. 15	$3d$ Heisenberg	Continuous renormalization group	0.37
Ref. 16	$3d$ Heisenberg	Field theory: $d=3$ expansion	0.3655 ± 0.0005
Ref. 17	$3d$ XY	Monte Carlo+High temp. expansion	0.3485 ± 0.0002
Ref. 18	$3d$ Ising	Field theory	0.325

Heisenberg model.¹⁴ These measurements suggest that the antiferromagnetism of this material can be described by the 3D Heisenberg model. This result supports the use of a Heisenberg Hamiltonian for modeling the AF ordering in ordered Pt_3Fe alloys.⁷

In order to understand how epitaxial growth influences the critical exponents of $\text{Pt}_{73}\text{Fe}_{27}$, it is desirable to compare the present results of critical exponents with the critical exponents of the AF phase transitions in bulk $\text{Pt}_{73}\text{Fe}_{27}$. For this purpose, we have digitized the neutron diffraction data of Ref. 2 for the $\text{Pt}_{73.3}\text{Fe}_{26.7}$ single crystal, whose composition is almost the same as the composition of the alloy in our film, and extracted the magnetization critical exponents β for the two magnetic phase transitions. The square root of the digitized counts are assigned as the standard errors on the neutron Bragg diffraction intensities. It is reasonable to compare the properties of our film with the $\text{Pt}_{73.3}\text{Fe}_{26.7}$ single crystal, since there is 1% uncertainty in the measurements of the composition of the film. The analysis procedure, described above, yielded $T_{N1} = 160.24 \pm 0.2$ K and $\beta = 0.40 \pm 0.03$ for the Q_1 phase. We find that the T_{N1} value of the film and the T_{N1} value of the single crystal are the same within the experimental uncertainties. The exponent in the single crystal is also in agreement with the result of the exponent found in the $\text{Pt}_{73}\text{Fe}_{27}$ film and with the predictions of the 3D Heisenberg model.^{14–16} The lower integrated intensity in the experiments of Ref. 2 are responsible for the larger uncertainty in the exponent found in the single crystal.

Similarly, the best fit to the digitized neutron diffraction data of Ref. 2 returned $T_{N2} = 116.7 \pm 0.2$ K and $\beta = 0.39 \pm 0.03$ for the Q_2 phase in $\text{Pt}_{73.3}\text{Fe}_{26.7}$ single crystal. Therefore, the T_{N2} value in the film is about 18% lower than the value found in the single crystal. The reduction of the spin reorientation transition temperature in the film could be associated with different grain sizes in bulk and in the film. It would be desirable to know the properties of this transition in the film as a function of the grain size that can be controlled by the film parameters such as the seed layer thickness.

A detailed comparison of the magnetization critical exponent β for the two AF phases in the $\text{Pt}_{73}\text{Fe}_{27}$ film, in the

single crystal and the theoretical predictions for three dimensional model magnets is presented in Table I. The value of the exponent for the Q_2 AF phase in the single crystal and in the film are in agreement with each other and with the predictions of the $3d$ Heisenberg universality class. The agreement of the exponents in the film and in the bulk can be reconciled with the good lattice match of $\text{Pt}_{73}\text{Fe}_{27}$ film with the a -axis-oriented sapphire substrate.⁴ We would like to note that the experimental critical exponent values of $\beta = 0.368 \pm 0.013$ for the Q_1 phase and $\beta = 0.39 \pm 0.03$ for the Q_2 phase are within 1.5 standard errors of the predicted value of 0.3485 ± 0.0002 of the $3d$ XY model,¹⁷ therefore, we cannot conclusively rule out this model. The critical exponent values found for the Q_1 and Q_2 AF phases indicate very small or negligible anisotropy either in bulk or in the film of Fe-rich Pt_3Fe as can be expected for a material of cubic symmetry. The negligible anisotropy of the single crystal and the film is, therefore, an intrinsic property of the Fe-rich Pt_3Fe , i.e., $\text{Pt}_{73}\text{Fe}_{27}$ alloy. The critical exponent values for both bulk and the $\text{Pt}_{73}\text{Fe}_{27}$ film grown on a -axis sapphire are also similar to that of NiO, which is another low-anisotropy cubic antiferromagnet for which $\beta \sim 0.38$ was determined.¹⁹ Theoretical investigations of the critical behaviors of metallic cubic antiferromagnets would be desirable for comparing with the critical exponents of Fe-rich Pt_3Fe at the two AF phase transitions.

In conclusion, using neutron diffraction measurements in the range of 75–175 K, we have determined the Néel temperature and the magnetization critical exponent β of the two AF phase transitions with the wave vectors $2\pi/a(1/2 \ 1/2 \ 0)$ and $2\pi/a(1/2 \ 0 \ 0)$, in a (111)-oriented $\text{Pt}_{73}\text{Fe}_{27}$ film grown on an a -axis-oriented sapphire ($\alpha\text{-Al}_2\text{O}_3$) substrate. The spin reorientation transition temperature or T_{N2} in the film is found to be 18% less than the value in the bulk. The exponent in both the AF phases is in excellent agreement with exponents extracted from the neutron diffraction data of Ref. 2 for a $\text{Pt}_{73.3}\text{Fe}_{26.7}$ single crystal and with the theoretical predictions for the $3d$ Heisenberg universality class.

The authors would like to thank Prof. W. H. Butler for helpful discussions. This research work was supported by the US Department of Energy through Grant No. DE-

FG02-02ER45966 and the National Science Foundation Materials Research Science and Engineering Center program through Grant No. DMR-0213985. This work was also partly

supported by Oak Ridge National Laboratory, managed by UT-Battelle, LLC, for the US Department of Energy under Contract No. DE-AC05-00OR22725.

-
- ¹M. E. Fisher, *Rev. Mod. Phys.* **46**, 597 (1974)
- ²G. E. Bacon and J. Crangle, *Proc. R. Soc. London, Ser. A* **272**, 387 (1963).
- ³C. S. Severin, C. W. Chen, and C. Stassis, *J. Appl. Phys.* **50**, 4259 (1979).
- ⁴S. Maat, O. Hellwig, G. Zeltzer, E. E. Fullerton, G. J. Mankey, M. L. Crow, and J. L. Robertson, *Phys. Rev. B* **63**, 134426 (2001).
- ⁵R. L. Compton, M. J. Pechan, S. Maat, and Eric E. Fullerton, *Phys. Rev. B* **66**, 054411 (2002).
- ⁶L. Vinokurova, V. Ivanov, E. Kulatov, M. Pardavi-Horvath, and E. Svab, *J. Phys. (Paris), Colloq.* **49**, C8-117 (1988).
- ⁷N. I. Kulikov, E. T. Kulatov, and S. I. Yakhimovich, *J. Phys. F: Met. Phys.* **15**, 1127 (1985).
- ⁸Y. Tsunoda, D. Tsuchiya, and Y. Higashiyama, *J. Phys. Soc. Jpn.* **72**, 713 (2003).
- ⁹G. L. Squires, *Introduction to the Theory of Thermal Neutron Scattering* (Cambridge University Press, Cambridge, 1978).
- ¹⁰G. E. Bacon, *Neutron Diffraction* (Clarendon, Oxford, 1975).
- ¹¹S. W. Lovesey, *Theory of Neutron Scattering from Condensed Matter* (Oxford, New York, 1984), Vol. 2.
- ¹²J. W. Lynn, *J. Appl. Phys.* **75**, 6806 (1994).
- ¹³D. P. Belanger, J. Wang, Z. Slanic, S.-J. Han, R. M. Nicklow, M. Lui, C. A. Ramos, and D. Lederman, *Phys. Rev. B* **54**, 3420 (1996).
- ¹⁴M. Camprostrini, M. Hasenbusch, A. Pelissetto, P. Rossi, and E. Vicari, *Phys. Rev. B* **65**, 144520 (2002).
- ¹⁵G. v. Gersdorff and C. Wetterich, *Phys. Rev. B* **64**, 054513 (2001).
- ¹⁶F. Jasch and H. Kleinert, *J. Math. Phys.* **42**, 52 (2001).
- ¹⁷M. Camprostrini, M. Hasenbusch, A. Pelissetto, P. Rossi, and E. Vicari, *Phys. Rev. B* **63**, 214503 (2001).
- ¹⁸J. C. Le Guillou and J. Zinn-Justin, *Phys. Rev. B* **21**, 3976 (1980).
- ¹⁹C. F. van Doorn, P. de V. Du Plessis, *Phys. Lett.* **66A**, 141 (1978).